Contents

1 Controlling chaos in a high-dimensional continuous spatiotemporal model

Abstract

A method for controlling low-order chaotic behavior of continuous spatiotemporal systems is presented. The method is inherently continuous in its treatment of both physical space and time and of reconstructed phase space. A general controllability criterion is developed for determining the optimal points in reconstructed phase space at which to apply the feedback control. Both delay-coordinate phase space and non-delay coordinate phase space reconstruction are considered.

The method is demonstrated in a complex, realistic 3d PDE model that is used successfully for predicting El Niño events in the Equatorial Pacific. An unstable periodic orbit that involves an oscillation of the entire model Pacific ocean and atmosphere is stabilized using a feedback control applied to a single degree of freedom at a carefully chosen single "choke point" in space. It is emphasized that unlike the situation in simpler systems, no out-of-a-box algorithm can be universally applied to complex spatiotemporal systems. The successful control of such complex spatiotemporal systems may be achieved only if a detailed understanding the relevant dynamics is used in order to choose the optimal control variable and control point in space.

1.1 Introduction

There has been significant interest in recent years in the control of low-order chaotic dynamical systems using small systematic perturbations that lead to the stabilization of unstable periodic orbits (UPO) [1, 2, 3]. Controlling large- or infinite-dimensional systems, however, such as spatiotemporal systems that are governed by partial differential equations is still in its infancy [4, 5, 6, 7, 8, 9, 10, 11]. In this paper, we discuss in some detail the approach proposed in [12] for the control of spatiotemporal systems that are continuous in both space and time. We

then describe the application of the proposed method to the control of a complex model, composed of a spatiotemporal system of PDEs, that simulates the El Niño phenomenon in the Equatorial Pacific ocean and atmosphere.

Spatiotemporal systems often do not have an accessible adjustable system-wide parameter that can be used for an OGY [1, 11] control. In such systems it often makes more sense and is more practical to apply the control perturbation to one of the dynamical variables, at a specific spatial location. Accordingly, our approach does not require the existence of a global adjustable parameter; rather, it is based on applying OGY-like feedback perturbations to a single dynamical degree of freedom of the system [13], at a single point in space.

The spatiotemporal system successfully controlled here seems to be significantly more complicated than the previously controlled discrete systems of coupled chaotic elements [5, 7], or relatively simple or isotropic 1d or 2d systems of PDEs [4, 6, 8, 9]. Often, the precise dynamics responsible for the chaotic behavior of systems of such complexity, whether they are models or experimental systems, is not known. Therefore a practical control methodology should not depend on the details of the dynamics or on a manipulation of specific known analytic solutions of the governing system of equations. We therefore use phase space reconstruction for deriving and applying the control law, thus not requiring a knowledge of the detailed dynamics of the system [14]. Both delay-coordinate and non-delay phase space reconstruction are considered here, in an extension to the work presented in [12]. While a knowledge of the specific governing equations of the controlled system is not required by the present methodology, we emphasize that an understanding of the dynamics is, in fact, crucial. As will be seen below, the control of complex spatiotemporal systems may not be achieved using an out-of-the-box algorithm, but requires a good understanding of the relevant dynamics to determine some of the basic features of the control strategy.

Previous approaches to the control of continuous systems were often based on a projection of the dynamics onto a discrete map. Our approach, in contrast, controls the continuous spatiotemporal system using a continuous reconstruction of the UPO in phase space. It turns out that this continuous treatment is crucial as we consequently find that not every point on the continuous UPO may be used to apply the control (and therefore that not every projection to a discrete map may be used). We therefore present a novel general criterion for determining the controllability of phase space points along a given UPO.

The paper outline is as follows (readers interested only in the chaos-control methodology presented here and not in the specific application to El Niño can read only the sections marked here by an asterisk). We first (section 1.2) briefly review the relevant aspects of El Niño's dynamics (section 1.2.1) and the theories that attribute El Niño's irregularity to low order chaos (section 1.2.2). Next, the El Niño model used here is described in section (1.2.3). Section (1.3*) discusses the choice of control variable (i.e. the variable to which control perturbations are applied) and of control point in physical space (the point in space where the perturbations are applied to the control variable). The actual control algorithm is derived in section (1.4*). The issue of at which point in reconstructed phase space to apply the control corrections, or in other words a criterion for the controllability of phase

space points is derived in section (1.5*). The results of applying the proposed control scheme to the El Niño model are presented in section (1.6). Finally, section (1.7*) discusses an extension of the above ideas to phase space reconstruction not based on delay coordinates, and we conclude in section (1.8).

1.2 El Niño's dynamics and chaos

While we obviously do not propose here the control of actual El Niño events, we do show that chaos control in a realistic El Niño model can contribute to the understanding of El Niño's dynamics. El Niño events involve a wide-spread warming of the equatorial Pacific Ocean surface water (shown in Fig. 1.1 for the model in which chaos is controlled in this work). The warming events last a few months to a year, occur irregularly in time every 2-6 years, dramatically affect worldwide weather, and have important social and economic implications. El Niño, and a corresponding "Southern-Oscillation" of atmospheric pressure are together termed ENSO [15]. Recent theories [18, 17, 19, 20] attribute El Niño's irregularity to a low order chaos. We thus briefly describe now the relevant aspects of El Niño dynamics (section 1.2.1), survey El Niño chaos theories (section 1.2.2), and describe the structure of the El Niño model used here (section 1.2.3) before proceeding to the control algorithm.

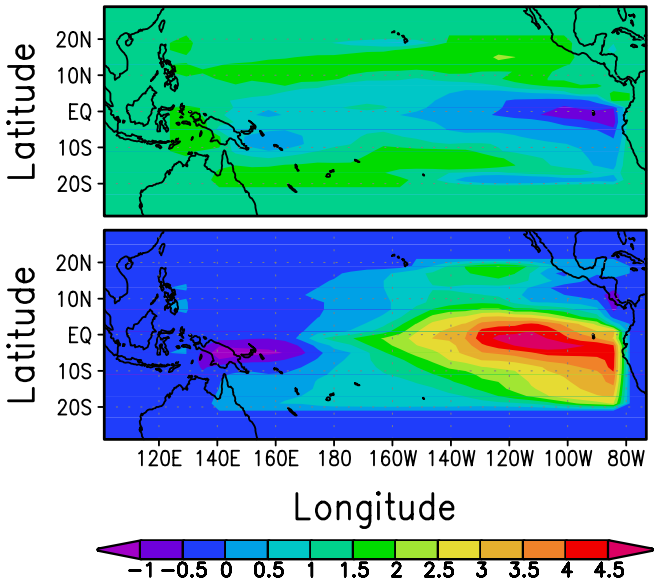

Fig. 1.1: The deviation of the sea surface temperature from its long-term mean during a peak of a model El Niño (warming) event (lower panel) and during the peak of a La Nina (cooling) model event (upper panel) which typically occurs between El Niño events.

1.2.1 El Niño's dynamics

Let us briefly examine the mechanism of the El Niño cycle, in a simplified version known as the "delayed oscillator" mechanism [23] (The "delayed" in "delayed-oscillator" has nothing to do with the delay-coordinate reconstruction of phase space, also used in this paper...). During non-El Niño periods, the wind along the Equatorial Pacific is easterly. The resulting wind-stress acting on the surface ocean water results in a "piling-up" of warm surface water on the western side of the basin where the sea-surface is therefore higher by a few tens of centimeters than in the eastern Pacific. As a result of this piling of warm water, the interface between the warm surface water and cold deep water (known as the thermocline) is also about 100 meters deeper in the western Pacific than in the eastern Pacific ocean. The sea surface temperature (SST) is warmer in the west Pacific ocean, and the east-west SST gradient drives the easterly winds.

El Niño events result from an instability of this basic state. The instability and positive feedback that causes it could be triggered by a number of factors, and we describe one possible (yet not unique) simple scenario here. Consider a weakening of the easterly winds in the central equatorial Pacific. The weakening results in a change to the wind stress curl which causes warm water to shift from higher latitudes towards the equator, creating an excess of warm water (i.e. a thermocline deepening) at the equator and of cold water (i.e. a thermocline shallowing) off the equator [23]. The equatorial thermocline deepening, in turn, increases the distance of the deep cold water from the surface and therefore weakens the mixing of cold deep water with the warm surface water. This results in a warming of the surface water. This thermocline deepening perturbation at the equator propagates eastward as a "Kelvin wave", reaching the eastern boundary after about 1 month. This wave involves eastward-only propagating vertical movements of the thermocline, is restricted to the equatorial domain, and exists due to the Coriolis force [24]. Upon reaching the eastern boundary, the thermocline deepening signal induces a warm SST perturbation there as well. The warming of the eastern Pacific SST reduces the east-west SST gradient, and thus further weakens the easterly winds above the equator that are driven by this gradient, creating a positive feedback (i.e. a coupled ocean-atmosphere instability) that leads to a rapid warming in the eastern equatorial Pacific Ocean, starting an El Niño event.

Meanwhile, the initial shallow thermocline perturbations off the equator in the central Pacific, and the corresponding cold SST perturbations, travel westward as Rossby waves. (Rossby waves exist due to the variation of the Coriolis force with latitude, and have a westward phase velocity). The cold Rossby waves are then reflected at the western boundary as cold equatorial eastward-traveling Kelvin waves. Amplified again by the atmospheric feedback, these cold Kelvin waves reach the Eastern Pacific delayed by about 6 months after the original wind perturbation, and terminate the El Niño event.

This is an extremely simplistic view of the El Niño mechanism, but it would suffice for our purpose here. For a recent review of current ideas about the El Niño mechanism, see [26].

1.2.2 El Niño's chaos

The delayed oscillator mechanism for the ENSO cycle, and its various extensions proposed over the past few years have provided quite a satisfactory explanation for the onset, termination and cyclic nature of ENSO events. However, two basic ENSO characteristics that are still unexplained by these delayed oscillator theories are the irregular occurrence of ENSO events and their apparent partial locking to the seasonal cycle [27]. Figure 1.2 shows the observed sea surface temperature over more than a century, showing the irregularity of ENSO events with regard to both the periodicity of the events and to the amplitude and evolution of each event. Figure 1.3 shows that in spite of this irregularity, the large-scale East Pacific sea surface temperature warming of many of the events tend to peak towards the end of the calendar year. (Data for both plots are from the January 1993 version of the Global Ocean Surface Temperature Atlas (GOSTA) [16]).

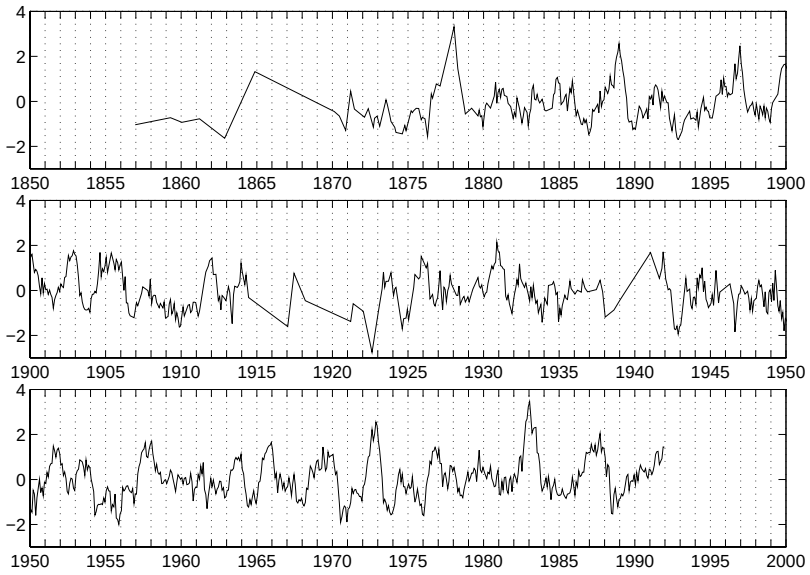

Fig. 1.2: The observed record of the NINO3 index (sea surface temperature anomaly averaged over 5°S–5°N and 90°W–150°W in the eastern Pacific), showing the irregularity of the events.

recent theories [19, 20, 18, 17] have proposed that the irregularity of ENSO may be explained as a low order chaotic behavior driven by the seasonal cycle. According to these ideas, ENSO is viewed as a periodically forced dissipative nonlinear oscillator (i.e. the delayed oscillator described above). As such, this system may undergo a transition to chaos according to the universal quasi-periodicity route to chaos [28]. The chaos arises because the natural delayed oscillator of the equatorial Pacific coupled ocean-atmosphere system can enter into a nonlinear resonance with

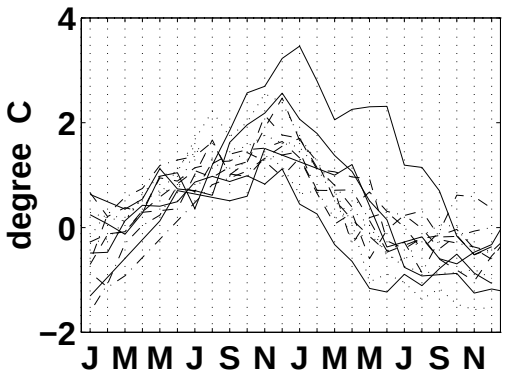

Fig. 1.3: Two-year segments of the observed NINO3 index (sea surface temperature anomaly averaged over 5°S–5°N and 90°W–150°W in the eastern Pacific) during observed ENSO events. The plotted segments begin at January of the years 1888, 1896, 1902, 1911, 1925, 1930, 1951, 1957, 1963, 1965, 1972, 1976 and 1982.

the seasonal cycle at different periods of the oscillator (mostly 2-5 years). In the chaotic regime, each of these nonlinear resonances constitutes an unstable periodic orbits in phase space. The coexistence ("overlapping") of these unstable resonances results in chaotic behavior due to the irregular jumping of the system between the different resonances (unstable periodic orbits). Fig. 1.4 shows several analyses of a time series from the fairly realistic El Niño model whose chaos is controlled in this work. The model is further described in the following section. The time series analyzed in Fig. 1.4 is from a model run using the standard parameter regime where the model is chaotic. The dimension of the attractor was estimated to be about 3.5 [19], so that the behavior is low-order in spite of the many formal degrees of freedom in this continuous spatiotemporal model.

The quasi-periodicity route to chaos involves a transition, as the system's nonlinearity is increased, from a periodic behavior with a period that is not commensurate with the forcing period (which in this case is the annual period) to a mode-locked regime characterized by a periodic solution with a period that is commensurate with the forcing period, to a chaotic behavior. In the model used here, this transition may be seen in model experiments as the strength of the seasonal cycle is increased, or as the coupling strength between the ocean and the atmosphere is increased. Fig. 1.5 shows a model run in which the coupling strength between the ocean and the atmosphere is reduced (and hence so is the model nonlinearity), and the solution is therefore mode-locked (in a stable nonlinear resonance, or equivalently, in a stable periodic orbit) at a perfectly periodic solution with a four year period (which therefore commensurate with the annual forcing frequency at a ratio of 4:1) rather than chaotic. Fuller description of this transition to chaos may be found in [20]. The significant role played in this scenario by the seasonal cycle provides also a simple explanation for the locking of ENSO events to the seasonal cycle (yet not a detailed mechanism, which is proposed in [29]).

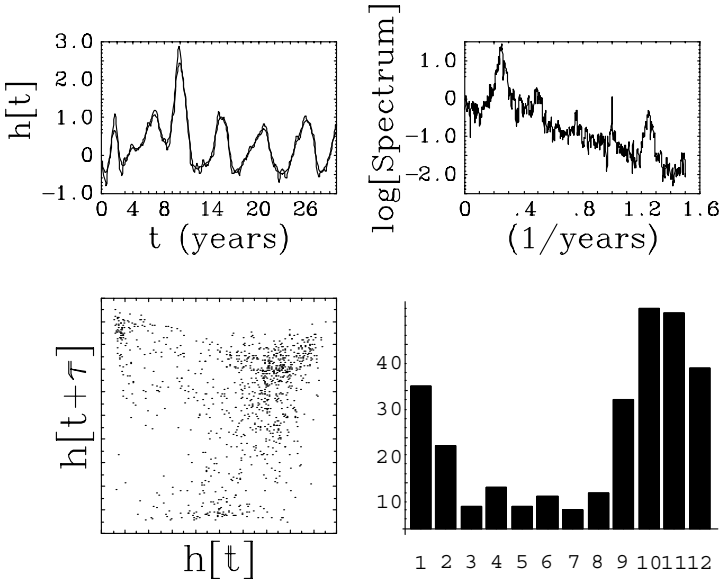

Fig. 1.4: Analyzes of the model NINO3 index time series for the standard seasonally forced chaotic model run. (a) A 30 year portion of the model NINO3 time series (thin line) showing the irregularity of El Niño events, and its 12-months running average (thick line). (b) Power spectrum characterized by a wide peak around 4 years. (c) A 2d reconstructed delay coordinate phase space Poincare-section obtained by subsampling the NINO3 time time series every year, using a delay $\tau = 1$ year. (d) A histogram of the number of ENSO events (vertical axis) per month of the calendar year (horizontal axis), showing the tendency of most events to peak towards the end of the calendar year, as for observed events.

The above chaos mechanism due to the periodic seasonal forcing is an attractive explanation for ENSO's irregularity, yet not the only possible one. It is possible, of course, that random excitations in the form of stochastic forcing of the large-scale delayed oscillator dynamics are the cause of the irregularity of ENSO events. The stochastic forcing could be due to short term weather phenomena which may be regarded as a random noise source for the large-scale dynamics because it results from processes that act on very short time scales of a few days and relatively small spatial scales. It is also possible that the large scale dynamics is chaotic even without the seasonal forcing. In fact, the ENSO model in which chaos is controlled in this study is sufficiently nonlinear that it is also (weakly) chaotic in the absence of a seasonal forcing as demonstrated in Fig. 1.6.

The chaos mechanism in this El Niño model seems to be chiefly due to the forcing by the seasonal cycle, so that with the periodic forcing present, the model irregularity is enhanced. Below, we shall demonstrate the control of the weakly chaotic model of Fig. 1.6 without the seasonal cycle.

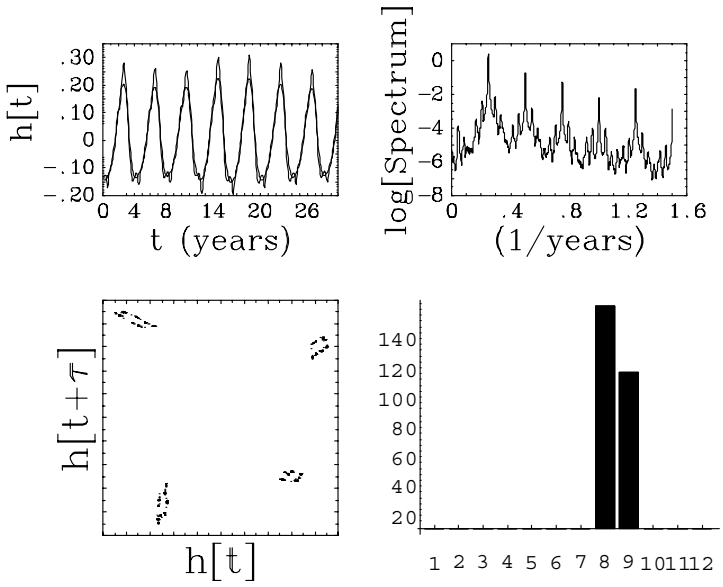

Fig. 1.5: Same as Fig 1.4, for the case of a weaker specified nonlinearity, where the model solution becomes mode-locked at a four-year nonlinear resonance with the seasonal cycle. The Poincare section reduces to four clouds corresponding to the four year period. The evolution of El Niño events is strongly coupled to the annual cycle and event peaks all occur in August-September. The spectrum is composed of sharp peaks at the main frequency of 4 years and its harmonics with the annual forcing frequency.

1.2.3 Model description

The El Niño model used here (described in detail in [21]) has proven quite successful in predicting El Niño events up to one and a half years in advance [22]. It is based on a set of nonlinear partial differential equations for the ocean and another one for the atmosphere, with specified couplings between them. The equations are written for the deviations from the observed spatially-variable long-term mean state of the Equatorial Pacific. This mean state may be seasonally varying [21], and in the model version used here (Fig. 1.6) is set to the time-independent mean July state. In the model equations t is the time, (x, y, z) are the (east, north, up) coordinates; (u, v, w) the corresponding ocean water velocities; (u_a, v_a) the atmospheric wind velocity in the (east, north) directions; $\mathbf{v} = (u, v)$, $\mathbf{v}_a = (u_a, v_a)$; $\nabla = (\partial_x, \partial_y)$; the total depth of warm surface waters in the model, also known as the "thermocline" depth, is $h(x, y, t)$; $T(x, y, t)$ is the sea surface temperature (SST). $\overline{\mathbf{v}}$, $\overline{T}$ and $\overline{w}$ are the spatially variable specified observed long-term July mean fields; $\beta = df/dy$ is the gradient of the Coriolis parameter; and the terms with r, r_a and α represent various dissipation processes; H is a mean thermocline depth and g' denotes gravity acceleration. The model oceanic currents are driven by the atmospheric wind stress, $(\tau^{(x)}, \tau^{(y)})$, which is quadratically related to the

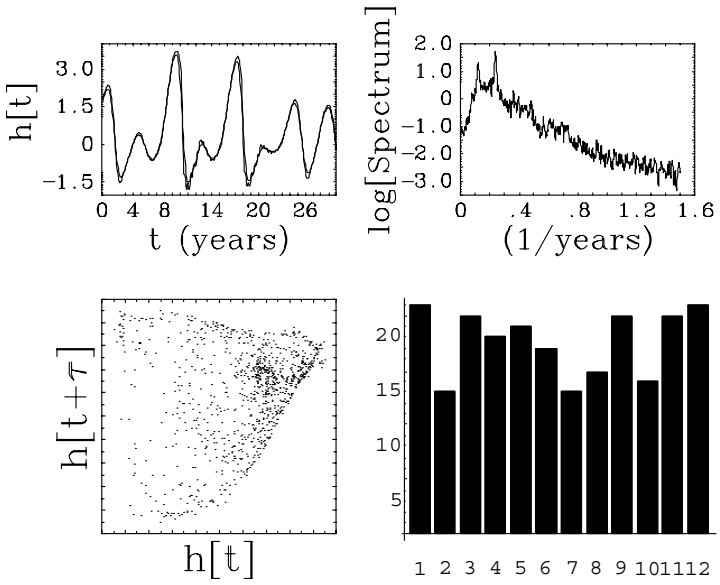

Fig. 1.6: Same as Fig 1.4, for the case of a perpetual July forcing (no seasonal cycle), where the model solution is weakly chaotic.

wind velocity (u_a, v_a). The atmospheric winds are driven by a heating, $Q[T, \nabla \mathbf{v}_a]$ which is a nonlinear function of the SST and of the atmospheric wind divergence. The model is composed of four sets of PDEs. The first set is for the vertically averaged ocean momentum and mass conservation equations,

$$\begin{aligned} u_t - \beta y v &= -g' h_x + \tau^{(x)}[u_a, v_a] - ru \\ \beta y u &= -g' h_y + \tau^{(y)}[u_a, v_a] - rv \\ h_t + H \nabla \mathbf{v} &= -rh. \end{aligned} \tag{1.2.1}$$

A second similar set of PDEs is used to simulate the vertical velocity shear in the ocean [21]. A third effectively 2d set of PDEs models the momentum and mass balances of the atmosphere,

$$\begin{aligned} \beta y v_a &= -\phi_x - r_a u_a \\ \beta y u_a &= -\phi_y - r_a v_a \\ \phi_t + H \nabla \mathbf{v} &= Q[T, \nabla \mathbf{v}_a] \end{aligned} \tag{1.2.2}$$

Finally, the SST is determined by a nonlinear advection - dissipation equation roughly of the form

$$T_t + \overline{\mathbf{v}} \nabla T + \mathbf{v} \nabla (\overline{T} + T) + w \overline{T}_z + (\overline{w} + w) T_z = -\alpha T \tag{1.2.3}$$

The model's finite-difference discretization is based on many thousands of grid point variables. The model solution is aperiodic (Fig. 1.6) and involves unstable

interactions between the ocean and the atmosphere, which are manifested through multiple spatial and temporal scales of all model fields. Yet, the previously demonstrated low-order temporally chaotic behavior of this model [19, 20] makes it a perfect candidate for testing chaos-control ideas in a complex, high dimensional, spatially extended system. The challenge, of course, is to control an UPO that represents the full-domain oscillation of the El Niño cycle without applying the chaos-control corrections at many spatial locations.

1.3 choosing a control variable and a control point in space

One of the main keys to controlling chaos in a complex spatiotemporal system using the approach suggested here, is the careful identification of the correct spatial point and degree of freedom (model variable or physical quantity in an experimental system) to which control corrections are applied, based on an understanding of the system's dynamics.

The variation of the Coriolis parameter with latitude (βy in (1.2.1)) results in the equator being a wave guide for trapped ocean wave modes which have the form $H_n(y/\ell)\exp(-\frac{1}{2}y^2/\ell^2)\exp i(kx-\sigma_n t)$, with H_n being the Hermite polynomial of order n, and where $\ell = 3.2$ degrees latitude. The mode $n = 0$ is the eastward propagating equatorial Kelvin Wave discussed in section (1.2.1), and the $n > 1$ modes are the westward propagating, off equatorial, Rossby modes ([24]). These equatorial ocean Kelvin and Rossby waves play a central role in El Niño's dynamics [15] as seen in section (1.2.1) above.

Now, as made clear by the delayed oscillator mechanism of ENSO, the western boundary of the ocean at the equator is a "choke point" which affects the entire tropical Pacific through the reflection of the Rossby waves into Kelvin waves [23]. Remember that it is this reflection of the Rossby waves that bring about the termination of the warming event. We therefore chose to control the entire Equatorial Pacific model ocean and atmosphere by applying small perturbations to the oceanic model fields at the western boundary ($x = x_w$) of the Pacific Ocean. Moreover, we choose the applied control perturbations to have the y-structure of the Kelvin mode. Because the Kelvin mode amplitude decays like $\exp(-\frac{1}{2}y^2/\ell^2)$ away from the equator, the control correction directly affects the oceanic model fields only in a very small region near the equator, at the western boundary. Furthermore, the perturbation structure implies that our control variable is the Kelvin mode amplitude at the western boundary only, $K_w(t)$. The model solution for the ocean fields, which is obtained numerically over the finite difference model grid, may be expanded in terms of the equatorial Kelvin and Rossby modes (which constitute a complete set of eigen functions for the ocean dynamics (1.2.1)). In terms of such an expansion, it is clear that we are modifying a single degree of freedom out of thousands which exist in the model.

This choice of a choke point may seem somewhat counter intuitive at first sight, because the warming induced by the El Niño events actually occurs in the eastern Pacific (Fig. 1.1), while we are trying to control it by making changes thousands

of kilometers away in the western most Pacific. However, this choice clearly makes sense once we bring into account the role of the wave dynamics and of the western boundary of the ocean in the delayed oscillatory mechanism. This choice is thus based on some 10 years of research into El Niño's dynamics, making it clear that one needs a good understanding of the dynamics of such complex spatiotemporal chaotic systems in order to successfully control them.

1.4 A continuous delay-coordinates phase space approach to controlling chaos in high dimensional, spatiotemporal systems

As the next step in applying our method to the control of chaos in this model, we identify its UPOs. The UPOs are determined in an N dimensional delay-coordinate phase space reconstructed from our control variable, which is the Kelvin wave amplitude at the western boundary. Note that the approach presented here is not limited to delay coordinate reconstruction, and the case of non-delay coordinate phase space reconstruction is discussed in section 1.7 below.

The phase space coordinates are thus the N-dimensional vectors

$$\mathbf{X}(t) = \{X_i,\ i = 1, ..., N\} = (K_w(t-(N-1)\tau), ..., K_w(t-\tau), K_w(t))^T, \quad (1.4.1)$$

where the last coordinate, X_N, is the present-time Kelvin wave amplitude to which the control corrections will be applied. To identify the UPOs for a given period p, we search for phase space points $X(t)$ that return to the same neighborhood after a period p, so that

$$||\mathbf{X}(t) - \mathbf{X}(t-p)|| < \epsilon \quad (1.4.2)$$

for some small ϵ. Using $\tau = 1$ year, and plotting the number of such close pairs as a function of p, the UPOs show up as peaks (Fig. 1.7a).

By actually plotting the close pairs of neighbors identified through the criterion (1.4.2) for a given period as dots in a three dimensional reconstructed phase space ($N = 3$), we can visualize the UPOs, and two such UPOs are shown in Fig. 1.7c,d. The first UPO corresponds to a relatively weak El Niño event with a period of 4.3 years, while the second corresponds to a strong event followed by a very weak one, repeating with a period of 7.83 years.

Next, an $N \times N$ linear map, M, is least-square-fitted to the model dynamics over a small neighborhood in phase space near a point that is located along the controlled unstable periodic orbit, and that serves as the control point in phase space. The linear map should map the phase space point $\mathbf{X}(t-p)$ to the state of the system at a time p later, $\mathbf{X}(t)$. The map M is therefore found by minimizing, via a least-square procedure, the following quantity,

$$J(M) = \sum_t ||\mathbf{X}(t) - M\,\mathbf{X}(t-p)||^2. \quad (1.4.3)$$

Given the map M, we calculate its eigenvectors and thus find its stable and unstable manifolds. The feedback control correction is now calculated so that when the

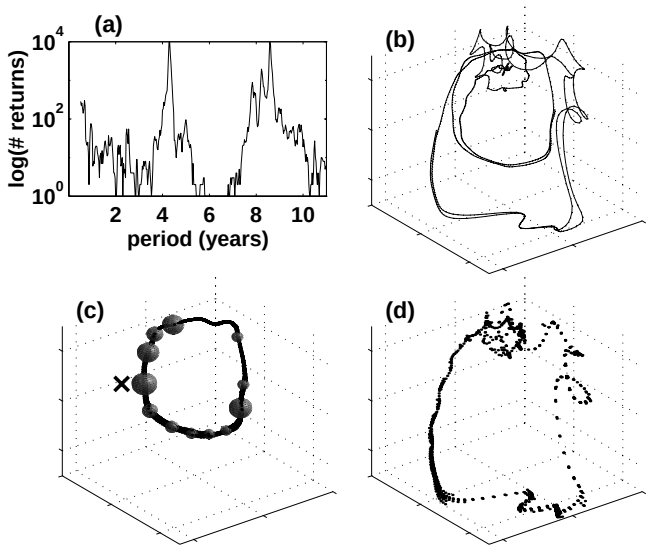

Fig. 1.7: (a) Log of number of near-returns as function of the period p. Each peak corresponds to an UPO, and the peak at $p = 4.3$ years is the one stabilized here. (b) A segment of phase space trajectory during a typical standard run, showing the trajectory switching between the two UPOs of panels (c) and (d). The three axes are $(K_w(t - 2\tau), K_w(t - \tau), K_w(t))$. (c) A 3d reconstructed delay coordinate phase space plot of the near returns forming the $p = 4.3$ years UPO that is stabilized in the controlled run. Larger balls along the UPO denote smaller G_{NN} and thus more controllable phase space points (see text). The most controllable phase space point, with the smallest G_{NN}, where the control correction is actually applied, is marked by "×". (d) An UPO with a period of $p = 7.83$ years.

system approaches the control point in phase space, the control correction brings the phase space trajectory $\mathbf{X}(t)$ towards the stable manifold of the UPO (see point $\mathbf{X}_2(t)$ in Fig. 1.8). By the definition of the stable manifold, the model evolution will then bring the trajectory of the control variable towards the UPO itself [1]. If our choice of a choke point in space is appropriate, the entire 3d model solution will follow the control variable and settle on the UPO as well.

We now derive the expression for the control correction in terms of the known location of the phase space point before the correction is applied, $\mathbf{X}(t)$, as well as the known stable and unstable eigenvectors of the map M. Suppose that the linear map M, evaluated at the control point, has N_s stable eigenvalues whose eigenvectors span the stable manifold. Let S be an $N \times N_s$ rectangular matrix composed of these N_s stable eigenvectors. Let $\mathbf{X}(t)$ be the phase space location of the model trajectory at time t, defined with the origin at the control point along the controlled UPO. The phase space location in the stable manifold to which we wish to bring the model trajectory can be written as $S\mathbf{a}$ where $\mathbf{a}$ is some $N_s \times 1$

coefficient vector. The control correction can only be applied to the present time Kelvin amplitude $K_w(t) = X_N(t)$, so that the phase space trajectory can only be corrected in the direction of a unit vector $\hat{\mathbf{X}}_N$ along the Nth axis in phase space. The phase space location after the application of the control perturbation δX_N is, therefore, $\mathbf{X}(t) + \hat{\mathbf{X}}_N \delta X_N$. We are interested in the control correction δX_N for which the distance of the corrected phase space location to the stable manifold, $d = ||S\mathbf{a} - (\mathbf{X}(t) + \hat{\mathbf{X}}_N \delta X_N)||$, vanishes. The amplitude of the correction, δX_N, is accordingly obtained by solving the equations requiring that the square of the distance d^2 to the stable manifold is minimized,

$$\partial d^2/\partial \mathbf{a} = \mathbf{0} \tag{1.4.4}$$

$$\partial d^2/\partial \delta X_N = 0. \tag{1.4.5}$$

Solving these $N_s + 1$ equations for the coefficient vector $\mathbf{a}$ and for the requested control correction amplitude δX_N we finally find

$$\delta X_N = (X_N - \hat{\mathbf{X}}_N^T G \mathbf{X})/(\hat{\mathbf{X}}_N^T G \hat{\mathbf{X}}_N - 1), \tag{1.4.6}$$

where $G = S(S^T S)^{-1} S^T$.

Given a time series from any spatiotemporal system, this simple control law may always be derived without additional knowledge of the dynamics. In the present case, we used $N = 3$ and found that typically there is one unstable eigenvalue of M (whose value, representing the amplification over a full orbit around the UPO, typically varies around 1.5), one neutral (value close to 1, and whose eigenvector points along the UPO) and one stable eigenvalue (< 1), so that we set $N_s = 2$.

The control correction (1.4.6) is applied to the control variable $X_N = K_w(t)$ when the phase space trajectory is within a small specified radius from the control point in phase space. But before displaying the results of a chaos-control experiment, we need to discuss the choice of a control point in phase space along the UPO to be stabilized.

1.5 Controllability of delay-coordinate phase space points along an unstable periodic orbit

One of our more generally applicable results here is a procedure for choosing the phase space points along a given UPO at which control may be applied. As explained above, our control correction is always applied in the direction of $\hat{\mathbf{X}}_N$ in the reconstructed phase space because this is the direction corresponding to the present-time control variable. If, for some control point, this direction is parallel to the stable manifold (Fig. 1.8), the control perturbations along $\hat{\mathbf{X}}_N$ cannot bring the phase space trajectory away from the unstable manifold.

Such an uncontrollable situation happens when the direction of $\hat{\mathbf{X}}_N$ is parallel to that of the stable manifold, which means that the unit-length vector $\hat{\mathbf{X}}_N$ may be written as a linear combination of the stable manifold eigenvectors, $\hat{\mathbf{X}}_N = S\mathbf{a}$, where $\mathbf{a}$ is a coefficient vector. Multiplying both sides of this equation on the left by

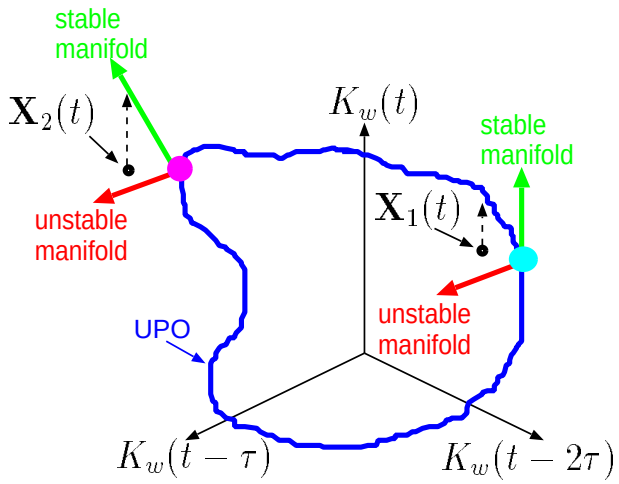

Fig. 1.8: A schematic drawing of an uncontrollable situation in which point $\mathbf{X}_1(t)$ cannot be brought towards the stable manifold using a control perturbation in the direction of $K_w(t)$. In contrast, $\mathbf{X}_2(t)$ is near a controllable point on the UPO, because a perturbation in the direction of $X_N = K_w(t)$ can bring $\mathbf{X}_2(t)$ towards the stable manifold along the thin dash arrow starting at $\mathbf{X}_2(t)$.

S^T and then by $(S^T S)^{-1}$ we obtain $(S^T S)^{-1} S^T \hat{\mathbf{X}}_N = \mathbf{a}$. Multiplying again on the left of each side by S, we find $S(S^T S)^{-1} S^T \hat{\mathbf{X}}_N = S\mathbf{a} = \hat{\mathbf{X}}_N$. Finally, multiplying by $\hat{\mathbf{X}}_N^T$ and using $\hat{\mathbf{X}}_N^T \hat{\mathbf{X}}_N = 1$, we find for an uncontrollable phase space point,

$$G_{NN} = \hat{\mathbf{X}}_N^T G \hat{\mathbf{X}}_N = 1. \tag{1.5.1}$$

This uncontrollability condition leads, according to (1.4.6), to an infinite amplitude correction δX_N. Likewise, a smaller G_{NN} implies a smaller perturbation δX_N required to bring $X(t)$ to the stable manifold, and thus a better phase space point to apply the control. Fig. 1.7c shows how the variation of G_{NN} along the stabilized UPO may be used to choose an appropriate control point in phase space.

This controllability condition may be extended to non-delay coordinates as discussed in section 1.7 below. We note that the above controllability condition only addresses one aspect of controllability, i.e. the direction of realizable perturbations vs the direction of the stable and unstable manifolds. Given many controllable points along the UPO to be controlled based on the condition that G_{NN} is as small as possible, one may need to apply additional considerations for the choice of the optimal control point. For example, one may bring into account the location of possible control points relative to the location of other UPOs that need to be avoided, or the amplitude of the local Lyapunov exponents of the stable and unstable manifold at different possible control points, etc.

1.6 Results

Let us examine the results of the application of the above control procedure to our El Niño model. During the model integration, the control correction δX_N is calculated using (1.4.6). The Kelvin wave amplitude at the western boundary of the Pacific is corrected by δX_N only when the model trajectory in phase space nears the control point, and only when δX_N is smaller than a pre-specified threshold. Fig. 1.9 shows the model solution with and without control, demonstrating that the procedure outlined here indeed works most efficiently for this complex El Niño model.

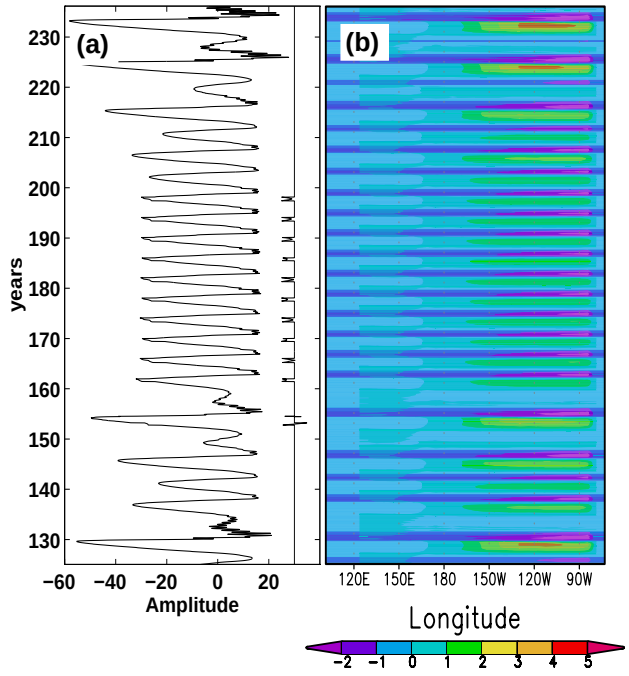

Fig. 1.9: (a) Left curve: a time series of the Kelvin wave amplitude on the western boundary of the Pacific Ocean, to which the control is applied from year 150 to 200. Right curve: the magnitude of the applied control perturbation (shifted to the right by 30 units so it would not overlap the other time series). (b) A plot of the equatorial sea surface temperature as a function of longitude and time during the same run. The controlled, periodic behavior during years 150-200 represents a full-domain oscillation of a complex spatial structure and temporal evolution.

Before the control procedure is turned on at time $t = 150$ years, the model is in its chaotic regime. After the control is turned on, the model trajectory in phase space approaches the control point on the UPO to be stabilized at year 153-

154 and a control corrections are applied twice, yet do not succeed in stabilizing the system on the UPO. Later, after year 160, the model again approaches the control point in phase space, and this time the control correction manages to trap the model evolution on the UPO. From that point onward to time $t = 200$ years, the control correction is applied every about 4.3 years, and the model evolution is perfectly periodic, as can be seen in both the time series of the Kelvin wave amplitude and the plot of the sea surface temperature along the entire equator. Once the control procedure is turned off at year 200, the model rapidly returns to its chaotic behavior.

A closer look at the control perturbation and model response during the control period is given in Fig. 1.10. One can see that the control perturbations are applied to the Kelvin wave amplitude at the western boundary of the Pacific Ocean when this wave amplitude is at its minimum. The control perturbations start when the sea surface warming in the east Pacific is at its peak, and are applied over a few months until near the end of the warming period.

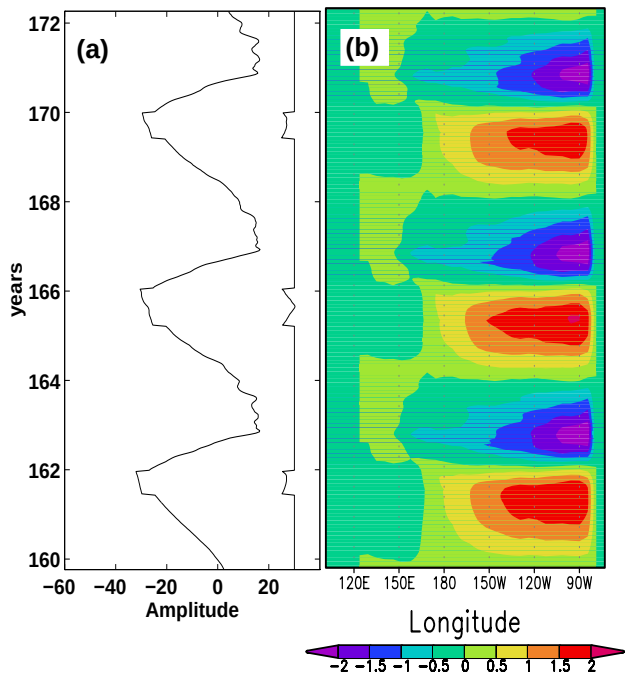

Fig. 1.10: Same as Fig. 1.9, zooming over a shorter time interval

We could not attribute any physical meaning to the timing of the perturbations. The timing of the control perturbations relative to the evolution of the controlled El Niño events is a consequence of the choice of the control point in phase space. This choice, in turn, is dictated by the limitations of realizable movements in phase

space to the direction of the present-time Kelvin wave axis, as discussed above.

There are some interesting implications of the successful control of chaos in this model to the understanding of El Niño's dynamics. Previous works debated whether the aperiodicity in the El Niño model used here is due to low-order chaos [19, 20], or due to "noise" expressed in the model as high frequency, small spatial-scale air-sea interactions in the western Pacific. This "noise" can be seen in Fig. 1.9a as an intermittent high frequency signal at years 130-135, for example [25]. The existence of unstable manifolds of the UPOs and the successful control of chaos in this El Niño model are a clear demonstration that the aperiodicity in this model is due to low-order chaos (whether El Niño events in the actual equatorial Pacific are aperiodic due to chaos or noise is still under debate).

Given that we have demonstrated that the high-frequency small-scale signal seen in the model is not the cause of the aperiodicity of the model El Niño events, we can proceed to speculate on the source of this signal. Each unstable spatiotemporal UPO in this system is, of course, characterized by both different temporal evolution and different spatial patterns. This leads to an especially interesting possibility that the small-scale, high-frequency "noise" in spatiotemporal systems (such as seen in the Western Pacific in this model) may be a result of the low-order chaotic behavior, due to the large-scale spatial fields readjusting when jumping from one UPO to another.

1.7 Using non-delay coordinates for phase space reconstruction

Delay coordinates are useful when one has access only to a single parameter within the observed or simulated system. Often, however, one can measure more than one parameter, and then a more complete set of observations may be used to reconstruct the phase space picture in a way that is more reliable than using delay coordinates based on a single measured quantity. The use of non-delay coordinates has implications both on the reconstruction of the UPOs, and on the controllability condition derived above.

As an example, we have repeated the calculation of the number of near-returns as function of a period using both delay coordinates and non-delay coordinates (see Fig. 1.7a). The non-delay coordinates phase space reconstruction was done using physically significant measures of the state of the El Niño cycle, that are expected to provide mutually independent information based on our understanding of the El Niño mechanism. More specifically, we have used as the reconstructed phase space coordinates the following physical variables: Kelvin wave amplitude in western Pacific; the NINO3 average sea surface temperature index (Fig. 1.2); the thermocline depth averaged over the same area as the NINO3 index; the thermocline depth averaged over the west equatorial Pacific; the thermocline depth averaged over the central Pacific south of the equator; and the thermocline depth averaged over the central Pacific north of the equator. Note that when using delay coordinates one is limited to a number of coordinates N such that the delay time $N\tau$ is not much larger than the decorrelation time of the system. In the El Niño model considered

here, this means a practical limit of about $N = 3$ to $N = 4$ with a coordinate delay time of one year. When using non-delay coordinates, this limit on the number of coordinates does not exist, and one may choose as many independent measures of the system state as the phase space coordinates as are available.

The calculation of number of near returns using both phase space reconstructions was done for both the weakly chaotic perpetual July model run (Fig. 1.6) that was controlled above and for the more strongly chaotic seasonal model run (Fig. 1.4). The results for the number of near returns as function of period are shown in Fig. 1.11. It is very clear that the non-delay coordinates provide a smoother and cleaner picture of the peaks in these plots and thus of the unstable periodic orbits of the model. In particular, using non-delay coordinates (Fig. 1.11b) one can see in the seasonal model the annual harmonics that are expected to be UPOs of the model, while they are hardly distinguishable in the delay coordinates calculation for the same model run (Fig. 1.11a).

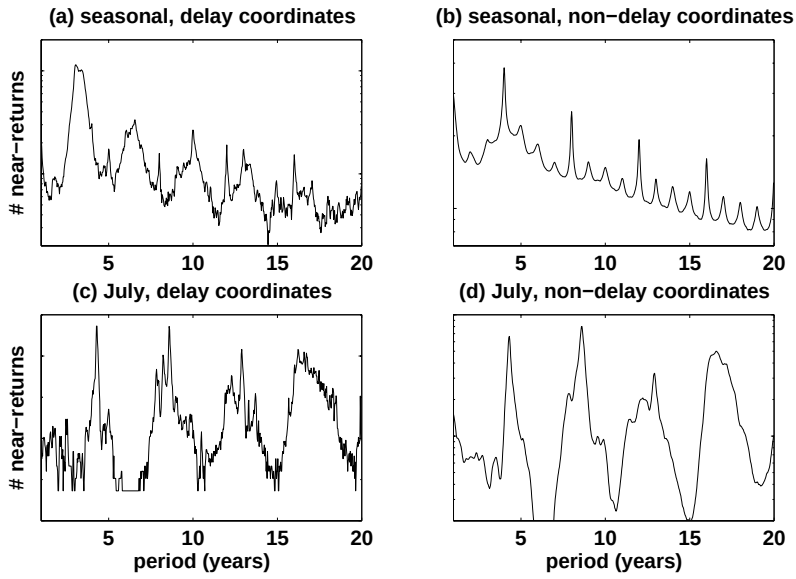

Fig. 1.11: log of number of near returns vs period: (a) seasonal model (strongly chaotic), delay coordinates, (b) seasonal model, non-delay coordinates, (c) perpetual July model (weakly chaotic), delay coordinates, (b) perpetual July model, non-delay coordinates,

Our controllability condition (1.5.1) may also have a different form when non-delay coordinates are used. It is possible, for example, that several parameters of the system may be measured in order to reconstruct the phase space trajectory and the UPOs, but that only a single parameter is accessible to control perturbations. In this case, this control parameter takes the place of X_N in our derivation, and the above control law and controllability condition are unchanged. If, however,

the number of parameters accessible for applying control perturbations is less than the number of parameters used for phase space reconstruction, yet is larger than one, then our above derivation for both the control law (1.4.6) and the controllability condition (1.5.1) needs to be generalized. The conceptual basis behind the derivation, however, is unchanged.

1.8 Conclusions

We have presented a procedure for controlling chaos in a continuous spatiotemporal system, and have demonstrated it by controlling the low-order weakly chaotic behavior of a realistic El Niño model that is used in actual prediction of El Niño events in the Equatorial Pacific ocean and atmosphere.

Rather than applying the control correction to a global adjustable parameter, the present method applies the perturbations directly to a dynamical degree of freedom of the model, as was done for simpler systems in [13]. In complex spatiotemporal systems, this requires a careful choice of the right dynamical variable to which to apply the corrections, as well as the spatial location in which this should be done. These two choices are most crucial, yet cannot be done according to some generic algorithm, but rather must be based on a good understanding of the relevant dynamics.

The control method proposed here is inherently continuous in its treatment of space, time and phase space, and is not built around a projection of the dynamics to a discrete map. Thus a continuous UPO is first identified in a reconstructed phase space, and then a point on the UPO at which perturbations are to be applied is chosen. We have found that this point on the UPO cannot be chosen arbitrarily and have formulated a criterion for this choice, based on the direction of stable manifolds of the UPO relative to the direction of realizable control corrections in phase space. While most of the work here was based on delay-coordinate phase space reconstruction, we have also considered a non delay-coordinate phase space reconstruction, and demonstrated that when such a reconstruction is feasible (when more than one measurable parameter exists in the system), it has some advantages over the delay-coordinate approach.

By controlling chaos in a realistic El Niño model we were able to gain some useful insights regarding El Niño's chaos. There is also an interesting lesson regarding spatiotemporal systems in general. Unlike fully developed turbulence, low-order chaotic behavior in a spatiotemporal system with many degrees of freedom typically involves the active participation of only the larger spatial scales and slower temporal scales of the system. We have seen, however, that the low-order chaos in our spatiotemporal model involved some high-frequency, small scale signal as well. Generally, each UPO is characterized by a unique large spatial scale structure, and slow temporal evolution. We have speculated that high frequency, small scale signals in such systems may be a result of low-order behavior, due to the large-scale spatial fields readjusting when the system jumps from one UPO to another.

The successful application of the chaos control method presented here to a complex PDE El Niño model is a clear demonstration of the robustness and potential of

the method. In addition, the results presented here may also contribute to the important problem of understanding and predicting El Niño events in the Equatorial Pacific.

Acknowledgments: I thank Steve Zebiak and Marc Cane for helping with the use of their model, and J. York for his suggestion to examine the non-delay coordinate reconstruction. This research was partially supported by the Israel-US Binational Science Foundation.

Bibliography

[1] E. Ott, C. Grebogi, and J. Yorke, *Phys. Rev. Lett.* **64**, 1196 (1990).

[2] T. Shinbrot, *Advances in Physics*, **44** 73-111, (1995).

[3] L. W. Ditto, M. L. Spano, J. F. Lindner, *Physica D* **86**, 198-211, (1995).

[4] I. Aranson, H. Levine, L. Tsimring, *Phys. Rev. Lett.*, **72** 2561-4 (1994).

[5] D. Auerbach, *Phys. Rev. Lett.* **72**, 1184, (1994).

[6] C. Lourenco, M. Hougardy, A. Babloyantz, *Phys. Rev. E*, **52**, 1528-1532, (1995).

[7] A. Babloyantz, C. Lourenco, J. A. Sepulchre, *Physica D*, **86**, 274-283, (1995).

[8] Y. Braiman, J. F. Lindner, W. L. Ditto, *Nature*, **378**, 465-467, (1995).

[9] G. Hu, Z. Qu, K. He, *Int. J. Bifurcation and Chaos*, **5**, 901-936, (1995).

[10] M. Kushibe, Y. Liu, J. Ohtsubo, *Phys. Rev. E*, **53**, 4502-4508, (1996).

[11] M. Ding, W. Yang, V. In, W. L. Ditto, M. L. Spanno, B. Gluckman, *Phys. Rev. E.* **53** 4334-4344, (1996).

[12] E. Tziperman, H. Scher, S. Zebiak and M. A. Cane: *Physical Review Letters* **79**, 6, 1034-1037. (1997)

[13] A. Garfinkel, M. L. Spano, W. L. Ditto, J. N. Weiss, *Science*, **257**, 1230-1235, (1992).

[14] U. Dressler and G. Nitsche, *Phys. Rev. Lett.* **68**, 1-4 (1992).

[15] S. G. Philander, *El Niño, La Niña, and the Southern Oscillations* (Academic Press, San Diego, California, (1990).

[16] Bottomley M., C. K. Folland, J. Hsiung, R. E. Newell, and D. E. Parker. Global ocean surface temperature atlas "GOSTA". Meteorological Office, Bracknell, UK and the Department of Earth, Atmospheric and Planetary Sciences, Massachusetts Institute of Technology, Cambridge, MA, USA. 20 pp and 313 plates. (1990).

[17] Chang P., B. Wang., T. Li, L. Ji., *Geophys. Res. Let.*, 21, 2817-2820, (1994).

[18] Jin, F-F, D. Neelin and M. Ghil, *Science*, **264**, 70-72, (1994).

[19] Tziperman E., L. Stone, M. A. Cane and H. Jarosh, *Science*, **264**, 72-74, (1994).

[20] Tziperman, E., M. A. Cane and S. Zebiak, *J. Atmos. Sci.*, **52**, 293-306, (1995).

[21] Zebiak, S. E. and M. A. Cane, *Mon. Wea. Rev.* **115**, 2262 (1987).

[22] M. A. Cane, S. E. Zebiak, and S. C. Dolan, *Nature*, **321**, 827 (1986). D. Chen, S. E. Zebiak, A. J. Busalacchi and M. A. Cane. *Science*, (1995).

[23] M. J. Suarez, and P. S. Schopf, *J. Atmos. Sci.* **45**, 3283 (1988); N. E. Graham and W. B. White, Science **240**, 1293 (1988); Battisti, D. S., J. Atmos. Sci., **45**, 2889, (1989).

[24] Gill, A. E. *Atmosphere-ocean dynamics*, Academic Press, Orlando, (1982).

[25] Mantua, J. N. and D. S. Battisti *J. Climate*, **8**, 2897-2927, (1995).

[26] Neelin, J. D., D. S. Battisti, A. C. Hirst, F.-F. Jin, Y. Wakata, T. Yamagata, S. Zebiak. Special Joint issue of J. Geophys. Res. Atmospheres and J. Geophys. Res. Oceans. In Press. (1998).

[27] Rasmusson, E., and T. Carpenter, *Mon. Wea. Rev.*, **110**, 354-384. (1982).

[28] Bak, P., T. Bohr and M. H. Jensen, *Physica Scripta*, **T9**, 50-58. (1985).

[29] Tziperman, E., M. A. Cane, S. Zebiak, Y. Xue, B. Blumenthal, **In press**, *J. Climate*, (1998).